J Mater Sci: Mater Electron (2017) 28:17405–17413
DOI 10.1007/s10854-017-7674-z

Binder-free polyaniline interconnected metal hexacyanoferrates nanocomposites (Metal = Ni, Co) on carbon fibers for flexible supercapacitors

M. A. Maier[1] · R. Suresh Babu[1] · D. M. Sampaio[1] · A. L. F. de Barros[1,2]

Received: 6 June 2017 / Accepted: 7 August 2017 / Published online: 16 August 2017

Abstract Improvement of the electrical conductivity, specific capacitance and binder-free polyaniline (PANI) interconnected with metal(II) hexacyanoferrate(III) (MHCF) nanocomposites (M = Ni, Co) on flexible carbon fibers (CF) were designed in our present research goal. PANI/MHCF/CF nanocomposites were prepared by one-step co-polymerization method. Electrochemical studies like cyclic voltammetry, galvanostatic charge–discharge and electrochemical impedance spectroscopy were analyzed. Under the optimized conditions, the nanocomposites demonstrated remarkable electrochemical performances as supercapacitor electrode with outstanding specific capacitances of ~725 F g^{-1} at a current density of 1 A g^{-1}, and retained ~325 F g^{-1} even at a high current density of 20 A g^{-1} in 0.5 M H_2SO_4 + 0.5 M Na_2SO_4 solution. The excellent cycling stability with capacitance retention of 80% after 1000 cycles may be a potential electrode material for future supercapacitor when its cycling stability and rate performance are addressed.

Electronic supplementary material The online version of this article (doi:10.1007/s10854-017-7674-z) contains supplementary material, which is available to authorized users.

✉ A. L. F. de Barros
ana.barros@cefet-rj.br

[1] Laboratory of Experimental and Applied Physics, Centro Federal de Educação Tecnológica Celso Suckow da Fonseca, Rio de Janeiro 20271-110, Brazil

[2] NASA Ames Research Center, Mail Stop 245-6, Moffett Field, CA 94035-1000, USA

1 Introduction

The massive depletion of fossil fuels and serious ecological problems owing to its rapid growth of population and its worldwide economical market were attracted at recent decades. Hence, the modern society needs the alternative energy to replace the fossil fuels and nuclear energy which is clean, renewable, cheap, safe and feasible [1, 2]. Recently, supercapacitors as one of the promising energy storage technology which have attracted tremendous attention owing to its fast charging/discharging, high power density and long cycle life [3]. Supercapacitors can be classified based upon energy storage mechanism namely, electrochemical double layer capacitors (EDLCs) and pseudocapacitors. The EDLCs stores energy through fast electrostatic adsorption of electrolyte ions at the electrode surface, whereas the pseudocapacitors stores energy on reversible Faradaic redox reactions at the electrode and electrolyte interface [2, 4]. Among various supercapacitor electrode materials, EDLCs based on carbonaceous materials [5, 6] and pseudocapacitors based on redox materials with metal oxides/hydroxides [7, 8], metal sulfide/metal oxide hybrid [9], metal hexacyanoferrates [10, 11] and conducting polymers [12]. Pseudocapacitor materials can provide a huge specific capacitance, which far exceeds to that of EDLCs based materials [7].

Transition metal(II) hexacyanoferrate(III) MHCFs are important class of polynuclear inorganic mixed-valence compounds and their general formula is $A_xM_yFe(CN)_{6.z}H_2O$. In this formula, A is a countercation, M stands for transition metal ions (M = Ni, Cu, Co, Mn etc.), and x, y, and z are stoichiometric coefficients. From a structural viewpoint, MHCFs form a rigid three-dimensional cubic network of repeating –N≡C–Fe–C≡N–M–N≡C– units [13, 14]. Fe and M sites (lattice positions) are typically octahedral, and the zeolitic cavities (interstitial positions) are occupied by water

as well as countercations, which are necessary to achieve the charge neutrality. The zeolitic structure of Prussian blue (PB) and, generally, of MHCFs, permits the flux of different counter cations into the channels of the three-dimensional network, allowing some reversible redox reactions without any severe structural deformations. Due to its unique structure, MHCFs were extensively studied for its interesting electrochemical properties in various applications such as ion-exchange, chemical sensors, electrocatalysis, batteries and supercapacitors [10, 11, 13–19].

Polyaniline (PANI) has been considered as one of a promising conducting polymer, good redox reversibility, environmental stability, easy way, low cost of preparation and long time usage of pseudocapacitors [12, 20]. To achieve predominantly, during redox processes of PANI to maintain the charge neutrality through anion displacement and proton involvement from the supporting electrolyte [21, 22]. To control the redox properties of PANI and to make the processes even more stable when combining the functional composite (hybrid) based upon PANI and NiHCFs are used for electrochromic applications [23]. Hence, PANI is capable of incorporating negatively charged polynuclear species including Prussian blue type MHCFs [11, 13].

Binder-free fabrication of the supercapacitive electrode materials is a recent task for development of high performance supercapacitor devices without any binders and conductive carbon fillers. Hence, combination of these positively charged PANI with negatively charged MHCF as a composite (organic/inorganic hybrid) to make a binder-free electrode which also improves the specific capacitance for high performance supercapacitor. The present work reports the fabrication of PANI/MHCF nanoparticles decorated on flexible carbon fibers (CF) using simple one-step electrochemical method. The MHCF is alternatively interconnected with PANI on the CF as the highly conductive substrate, offering an excellent transportation of fast ion and electron transport. The attractive electrochemical property for supercapacitor electrode was confirmed by cyclic voltammetry, electrochemical impedance spectroscopy (EIS) and galvanostatic charge–discharge techniques. The PANI/MHCF/CF nanoparticles manifest ultrahigh capacitance and excellent cyclic stability at high rates.

2 Experimental procedure

2.1 Chemicals

Potassium ferricyanide, nickel sulfate, cobalt sulfate and sodium sulfate were obtained from Dinamica™. Polyaniline was purchased from Labsynth™. Carbon fibers were purchased from Barracuda™ Brazil. All other chemicals were of analytical grade and used as received without further purification. Double distilled water was used for all experiments.

2.2 Fabrication of PANI/MHCF/CF nanocomposite electrodes

Hundred and eighty micro liter (0.05 M) of aniline monomer, 0.05 M metal sulfate (M = Ni, Co) and 0.05 M potassium ferricyanide solution containing with 0.25 M Na_2SO_4 and 0.5 M H_2SO_4 electrolytes were kept in the electrochemical cell. The carbon fiber (1.0 cm × 1.0 cm) was electrochemically polymerized in the range between −0.2 and 1.0 V for 30 cycles at the scan rate of 50 mV s^{-1} (see supporting information Fig. S1). The PANI/MHCF/CF nanocomposites were dried in ambient temperature and washed with distilled water to remove the unbound materials on the electrode surface. The weight of the active material coated on the CF electrode surface was optimized at ~1.0 mg cm^{-2}. Figure 1a shows the snapshot of the bare CF electrode. The CF electrode was extremely flexible, highly conductive and mechanically strong. Figure 1b shows the picture of the electrodeposited PANI/MHCF/CF nanocomposite electrode.

2.3 Material characterization

The morphology of the fabricated PANI/NiHCF/CF and PANI/CoHCF/CF nanocomposite electrodes was analyzed using field emission scanning electron microscope (FESEM). FESEM image of the electrode surface was obtained on SU6600® (HITACHI, Japan). Atomic force microscope (AFM) (Nanosurf EasyScan 2®, Switzerland) was used for electrode surface analysis. Fourier transform infrared spectra (FTIR) of the supercapacitor electrode were obtained using FTIR spectrometer (Agilent Cary 630®, USA) in the range from 4000 to 400 cm^{-1}.

Electrochemical measurements were performed with IVUMSTAT instrument. The electrochemical analysis were carried out in 0.5 M H_2SO_4 + 0.5 M Na_2SO_4 electrolyte using a three-electrode cell comprising of platinum counter electrode, Ag/AgCl reference electrode and carbon

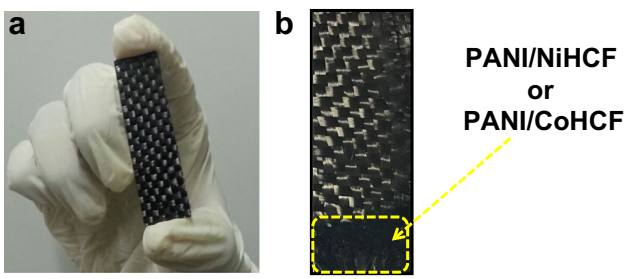

Fig. 1 **a** Photograph of the CF electrode; **b** electrodeposited PANI/MHCF/CF electrode

fiber (1 cm × 1 cm) electrochemically coated with PANI/MHCF nanoparticles as the working electrode. The cyclic voltammetric (CV) measurements were carried out in a cut off range between −0.2 and 1.0 V. The electrochemical impedance spectroscopy (EIS) measurement was carried out under open circuit potential between 0.01 Hz and 100 kHz. A two-electrode symmetric type cells were also utilized to investigate the specific energy and power of a single cell.

For three-electrode system, the galvanostatic charge–discharge property was measured at different current densities. The specific capacitances were calculated from galvanostatic charge–discharge with the following Eq. (1)

$$C = I\Delta t/m\Delta V \quad (1)$$

where C is the specific capacitance (F g^{-1}), I is the constant discharge current (A), Δt is the discharge time (s), m is the mass of active material within the electrode (mg) and ΔV is the potential range (V).

For the two-electrode system, also were measured the device capacitance (C) from galvanostatic charge–discharge based on the Eq. (1), where m is the total mass of active materials on both electrodes (mg) in the symmetric cell.

Specific energy density (ED, Wh/kg) and specific power density (PD, W/kg) can be obtained from the following Eqs. (2) and (3)

$$\mathrm{ED} = 1/2 \times C \times (\Delta V)^2 \quad (2)$$

$$\mathrm{PD} = \mathrm{ED}/\Delta t \quad (3)$$

3 Results and discussion

3.1 FTIR spectroscopy

Typical FTIR spectrum of the PANI/MHCF/CF nanocomposites electrodes are shown in Fig. S2 (see supporting information). The spectrum shows the characteristic peak of PB analogues [24]. A sharp stretching vibration peak of cyanide group (ν(CN)) around ~2083 and ~2087 cm^{-1} represents PANI/NiHCF and PANI/CoHCF respectively, which indicates the typical asymmetric CN vibration of ferricyanide [25]. It has been direct confirmation that the bridged binuclear of iron and metal ions (M = Ni or Co) species are coordinated through CN group in the nanocomposite electrode. Two peaks appeared at 1618, 1414 cm^{-1} (curve a) and 1644, 1404 cm^{-1} (curve b) corresponding to the ν(C=C) stretching vibration mode of benzene rings and ν(C=C) stretching vibration of the nitrogen quinine, respectively [11]. A broad peak around 3246 cm^{-1} observed for PANI/NiHCF and 3348 cm^{-1} corresponds to PANI/CoHCF show the stretching vibrations of the N–H group, indicating the formation of PANI in the nanocomposite. The broad adsorptive band occurring at approximately ~3378, 3387 cm^{-1} corresponds to the association of water due to the H-bonding; which is similar to that of PB [26].

3.2 Morphology of the PANI/NiHCF/CF and PANI/CoHCF/CF nanocomposite electrode

The surface morphology of the as-prepared PANI/NiHCF/CF and PANI/CoHCF/CF nanocomposites electrode along with CF electrode was investigated using FESEM. Figure 2 shows the FESEM images of CF, PANI/NiHCF/CF and PANI/CoHCF/CF nanocomposite electrode. From the Fig. 2a it can be clearly observed that the CF substrate was uncoated with a mere surface composed of number of tiny fibers. After electrodepositing, the PANI and MHCFs the CF surface was homogenously composed of spherical shaped MHCF nanoparticles embedded with PANI electrodeposited around the surface of CF electrode. The size distributions were in the ranges from 200 to 300 nm as shown in Fig. 2b, c.

AFM topographic 3D images of the CF, PANI/NiHCF/CF and PANI/CoHCF/CF nanocomposites electrode are shown in Fig. 3. The topographic images clearly displayed the CF electrode surface which is rougher with uneven islands, and the roughness increased from bare CF (uncoated) electrode to PANI/NiHCF/CF and PANI/CoHCF/CF nanocomposite

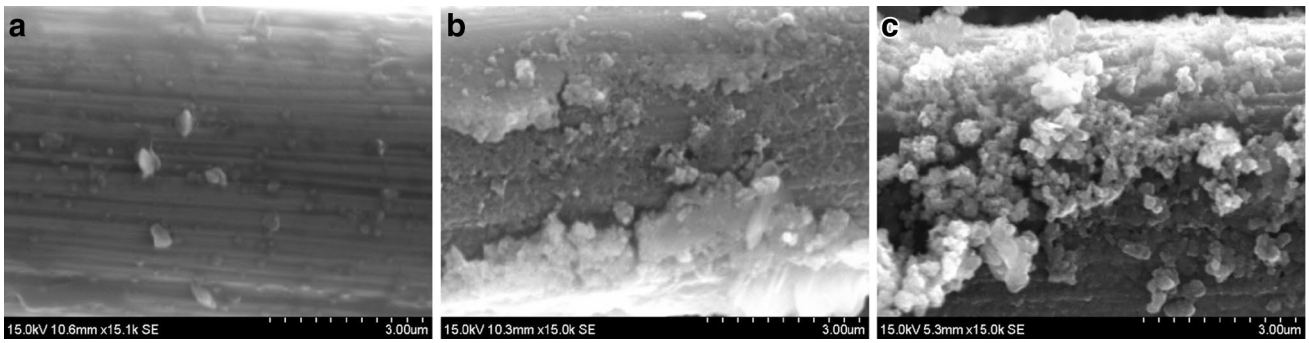

Fig. 2 FESEM images of **a** CF, **b** PANI/NiHCF/CF and **c** PANI/CoHCF/CF nanocomposite electrode

electrode. This clearly showed that the PANI/MHCF nanocomposites were uniformly deposited over the CF electrode surface. AFM analysis reveals the similar results of PANI/MHCF/CF nanocomposite electrodes as that obtained from the FESEM measurements.

3.3 Electrochemical characterization and supercapacitor performance analysis

The investigation of the electrochemical performance of the PANI/NiHCF/CF nanocomposite and PANI/CoHCF/CF nanocomposite electrodes were carried out through cyclic voltammetry (CV), galvanostatic charge–discharge technique and EIS in a three-electrode system. Figures 4 and 5 show the corresponding CV curves of the PANI/NiHCF/CF nanocomposite and PANI/CoHCF/CF nanocomposite electrode at different scan rates ranging from 2 to 50 mV s^{-1}. The CV curves exhibit a typical pseudo capacitance behaviour showing apparently three pairs of redox peak with the scanned potential for low scan rates as shown in Figs. 4a and 5a. The results and predictions were consistent with previous reports [11]. In briefly, the aniline is polymerized on

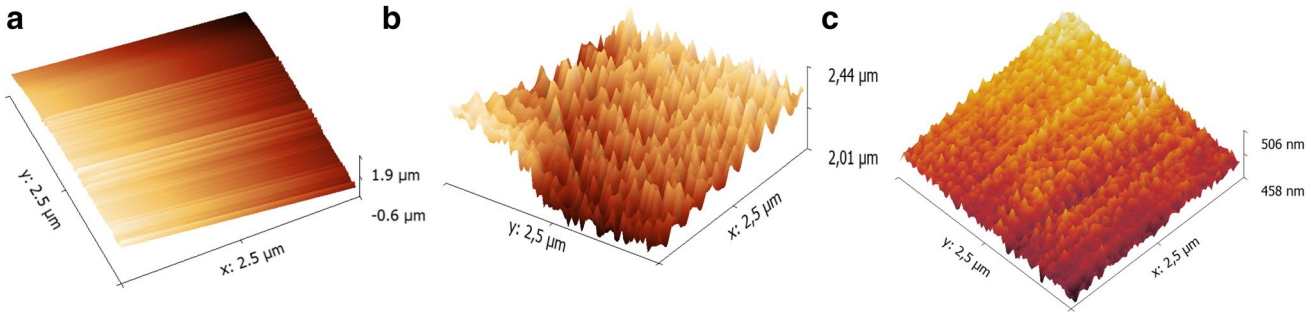

Fig. 3 AFM topographic images of **a** CF, **b** PANI/NiHCF/CF and **c** PANI/CoHCF/CF nanocomposite electrode

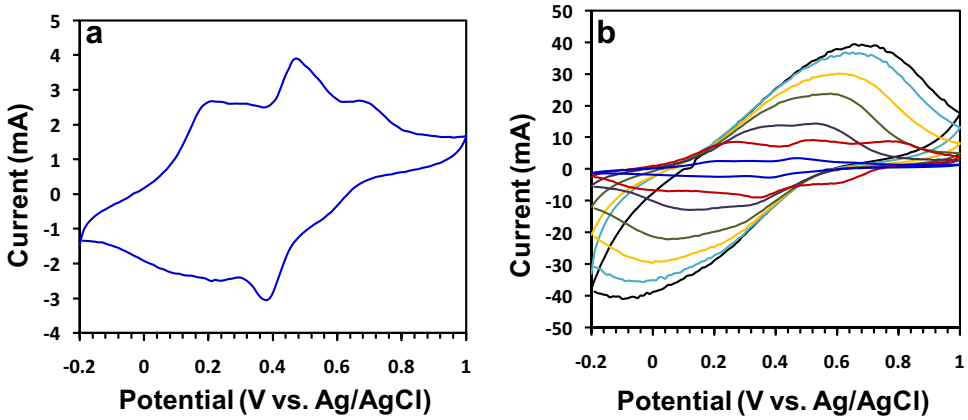

Fig. 4 **a** Cyclic voltammograms of PANI/NiHCF/CF nanocomposite electrode in 0.5 M H_2SO_4 + 0.5 M Na_2SO_4 electrolyte at the scan rate of 2 mV s^{-1} **b** Cyclic voltammograms of PANI/NiHCF/CF nanocomposite electrode at different scan rates from 2, 5, 10, 20, 30, 40 and 50 mV s^{-1}

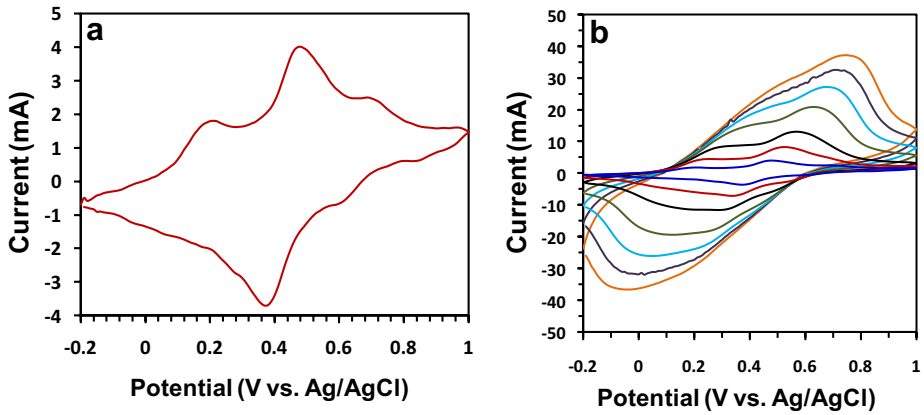

Fig. 5 **a** Cyclic voltammograms of PANI/CoHCF/CF nanocomposite electrode in 0.5 M H_2SO_4 + 0.5 M Na_2SO_4 electrolyte at the scan rate of 2 mV s^{-1}. **b** Cyclic voltammograms of PANI/CoHCF/CF nanocomposite electrode at different scan rates from 2, 5, 10, 20, 30, 40 and 50 mV s^{-1}

the CF electrode surface during positive scans, whereas the metal hexacyanoferrates are electrodeposited during negative scans. The organic/inorganic hybrids that are alternatively polymerized and deposited during cycling, might be interact electrostatically with each other because of partially oxidized PANI is positively charged and MHCF is anionic. This was identified from the CV, confirming the predictions. The first voltammetric redox peak at around −0.10 to 0.25 V is the characteristic peak of PANI. This corresponds to the reversible redox reaction of leucoemeraldine (insulating form) to emeraldine form (conducting form). Obviously next reversible redox reaction of Fe^{II} to Fe^{III} around the potential from +0.30 and +0.55 V corresponds to MHCF, for both NiHCF and CoHCF. The electron transfer reactions of MHCF are accompanied by insertion and exclusion of counter cation (Na^+) during reduction and oxidation respectively. The final redox peak around +0.55 and +0.80 V is assigned to the conversion of emeraldine to pernigraniline (fully oxidized form). The schematic illustration of oxidation and reduction mechanism for PANI/MHCF/CF nanocomposite electrodes is shown in Scheme 1.

Galvanostatic charge–discharge test was also applied to evaluate the electrochemical capacitive performance of PANI/NiHCF/CF and PANI/CoHCF/CF nanocomposite electrodes. Figure 6 shows the plot of potential versus time for PANI/NiHCF/CF and PANI/CoHCF/CF nanocomposite electrode at various current rates. A symmetric charge–discharge characteristic of triangular shape typical for ideal capacitor behaviour was observed even at high current density of 1.0 A g^{-1}, demonstrating fast charge propagation with no obvious IR drops and the curves had large deviation, demonstrating that the capacitance is mainly governed by the redox reactions of PANI and MHCF. With increasing current densities from 1 to 20 A g^{-1}, a very small IR drop in higher current densities was obtained. The specific capacitances were calculated from galvanostatic charge–discharge profiles. The capacitances fall between the lowest current density to highest current density were calculated for each sample and are presented in Table 1. Several conclusions can be drawn from these results. Firstly, PANI/NiHCF/CF and PANI/CoHCF/CF nanocomposites possess higher specific capacitances than that of pure MHCF electrodes and MHCF hybrid electrodes and the best performance is 718 and 723 F g^{-1} at 1 A g^{-1} of PANI/NiHCF/CF and PANI/CoHCF/CF nanocomposites respectively. A comparison of the specific capacitance obtained for PANI/NiHCF/CF and PANI/CoHCF/CF nanocomposites with the data reported for MHCFs hybrid electrodes are summarized in Table 2. The high capacitances might be caused by the tiny carbon fiber has high surface area which facilitates the

Scheme 1 Schematic representation of oxidation and reduction mechanism of PANI and MHCF nanocomposite

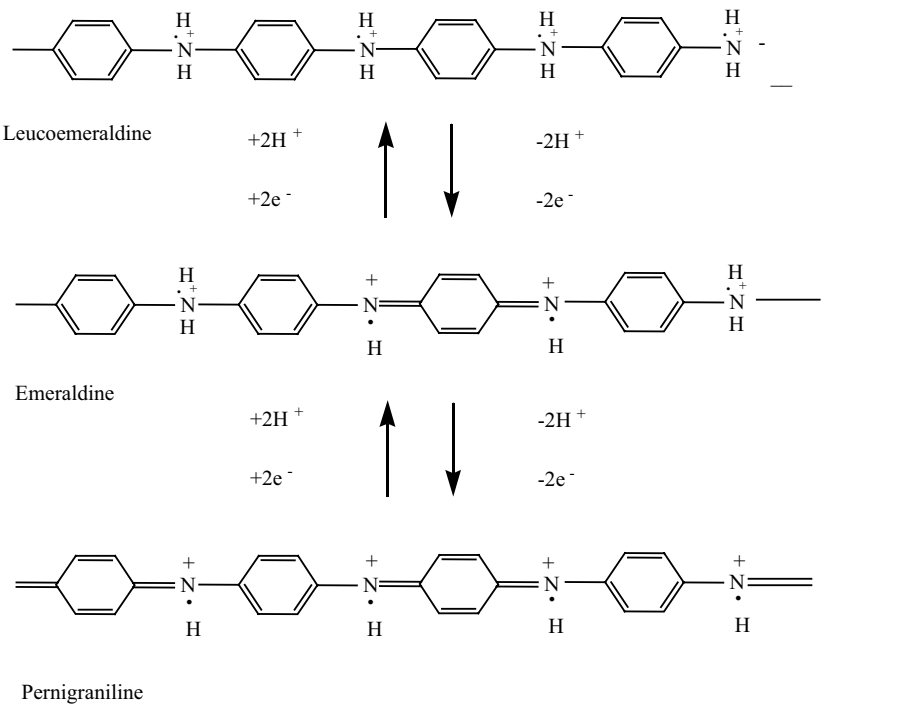

$$Na_2M^{II}[Fe^{II}(CN)_6 \longleftrightarrow NaM^{II}[Fe^{III}(CN)_6 + e^- + Na^+$$

M = Ni or Co

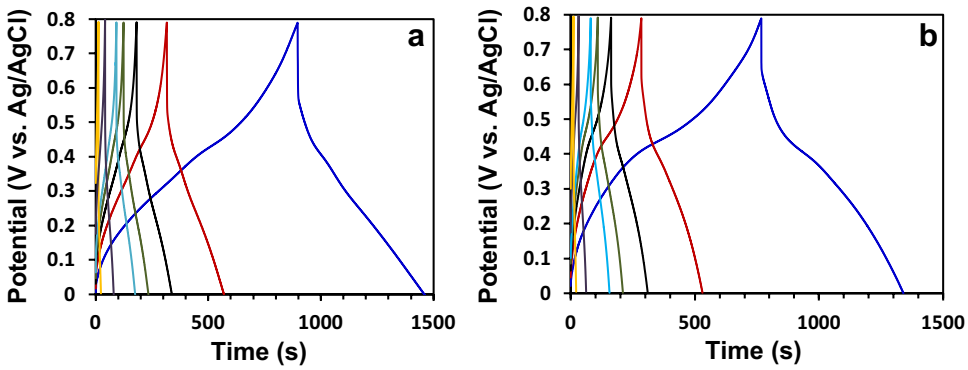

Fig. 6 Galvanostatic charge–discharge curves of **a** PANI/NiHCF/CF and **b** PANI/CoHCF/CF nanocomposite electrode with different current densities form 1 to 20 A g^{-1}

Table 1 Specific capacitances of PANI/NiHCF/CF and PANI/CoHCF/CF nanocomposites at different current densities

Current density (A g^{-1})	Specific capacitance (F g^{-1})	
	PANI/NiHCF/CF	PANI/CoHCF/CF
1	718	723
2	650	625
3	604	558
4	570	515
5	531	475
10	437	387
20	325	300

contact of the electrolyte in the surface of the PANI/MHCF nanocomposites.

The long-term cyclic stability of the PANI/MHCF/CF was evaluated in this study by repeating the galvanostatic charge–discharge test from 0 to 0.8 V at a current density of 5 A g^{-1} for 1000 cycles. The specific capacitances based on the electroactive materials as a function of cycle number are shown in Fig. 7. As seen from the Figure the PANI/NiHCF/CF and PANI/CoHCF/CF nanocomposite electrode exhibited high stability with slight decrease in the capacitance in the charge storage over the entire cycle numbers. The specific capacitance of the device initially increases and then becomes almost constant. After 1000 cycles, the capacitance decreases only around 20% of initial capacitance, exhibiting excellent cycle stability. The decrease of specific capacitance could be attributed due to the swelling and shrinkage of PANI during the long-term charge–discharge processes [31]. This high stability over long cycles demonstrates that the fabricated PANI/MHCF/CF electrode is suitable for practical applications.

To examine the primary behavior of the electrode materials for supercapacitors, EIS analysis was carried out using the Nyquist plot, EIS data were analyzed, which demonstrate the frequency response of the electrode/electrolyte system and are generally plotted against the impedance of the real component (Z') versus imaginary component (Z''). The Nyquist plots are usually interpreted by fitting the experimental data by an equivalent electrical circuit. Figure 8a, b shows the fitted Nyquist plots of PANI/NiHCF/CF and PANI/CoHCF/CF. The first intercepts of the semicircle with the real axis and the value of both ohmic resistance of the electrolyte and the internal resistance electrode materials and are represented as solution resistance (R_s). The semicircle in the high frequency region can be represented by an

Table 2 Comparison of specific capacitance of PANI/NiHCF/CF and PANI/CoHCF/CF nanocomposite supercapacitor electrodes with literature data

Electrodes	Cell configuration	Electrolyte	Working electrode	Current density (A g^{-1})	Specific capacitance (F g^{-1})	Refs.
CoHCF	3-electrode	0.5 M Na_2SO_4	Nickel foam	1.0	250.0	[10]
Ni/CoHCF hybrid	3-electrode	1.0 M KNO_3	Steel mesh	0.2	765.0	[27]
Co/MnHCF hybrid	3-electrode	0.1 M KNO_3	Glassy carbon	1.0	350.0	[28]
MnHCF nanocubes	3-electrode	1.0 M K_2SO_4	Nickel foam	1.3	690.0	[29]
NiHCF/PDDA/rGO	3-electrode	0.5 M Na_2SO_4	Glassy carbon	0.2	1320.0	[30]
PANI/NiHCF/s-CNT	3-electrode	1.0 M KNO_3	Pt sheet	2.0	430.7	[11]
PANI/NiHCF	3-electrode	0.5 M Na_2SO_4 + 0.5 M H_2SO_4	Carbon fiber	1.0	718.7	This work
PANI/CoHCF	3-electrode	0.5 M Na_2SO_4 + 0.5 M H_2SO_4	Carbon fiber	1.0	723.8	This work

interfacial charge transfer resistance (R_{ct}), and the straight line having a slope of 45° in the medium frequency signifies the Warburg resistance (W_d) and the pseudocapacitance C_P. The appropriate equivalent circuit for PANI/NiHCF/CF and PANI/CoHCF/CF is shown in Fig. 8c, and their fitting data are summarized in Table 3. The lowest R_s value was obtained for both PANI/MHCF/CF electrodes and specifies the excellent conductivity and also very high specific capacitance. The electrodes also attained the very low R_{ct} and W_d value. The lowest value for W_d signifies a short diffusive path of the electrolyte ions within the nanocomposites. The main theme for a supercapacitor is the frequency factor (n), which can explain the ideality of a composite toward supercapacitive behavior. The values of n differ between 0 and 1: $n=0$ indicate the resistor; $n=1$ indicates the ideal capacitor. The PANI/MHCF nanocomposites electrodes showed moderate supercapacitor behavior and achieved the highest n value of 0.70.

In order to further investigate, the capacitive performance of the symmetric PANI/NiHCF/CF and PANI/CoHCF/CF electrodes in a two-electrode system was performed. Figure 9 shows the typical galvanostatic charge–discharge curves of each symmetric supercapacitor [PANI/NiHCF/CF (Fig. 9a) and PANI/CoHCF/CF electrodes (Fig. 9b)]. The curves were measured as the current density varies from 0.5 to 5 A g^{-1} in 0.5 M H_2SO_4 + 0.5 M Na_2SO_4. The charge–discharge curves evidently displayed good symmetrical and linear in the cell voltage range from 0 to 0.7 V, which can be

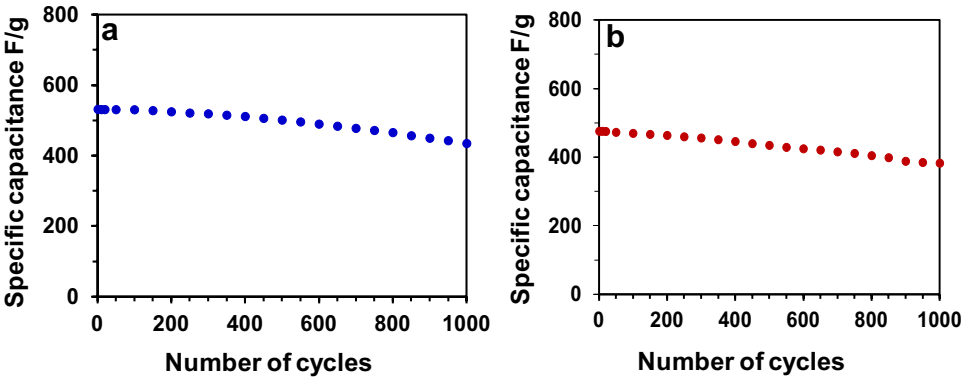

Fig. 7 Cycling stability curve of **a** PANI/NiHCF/CF and **b** PANI/CoHCF/CF nanocomposite electrode at a current density of 5 A g^{-1}

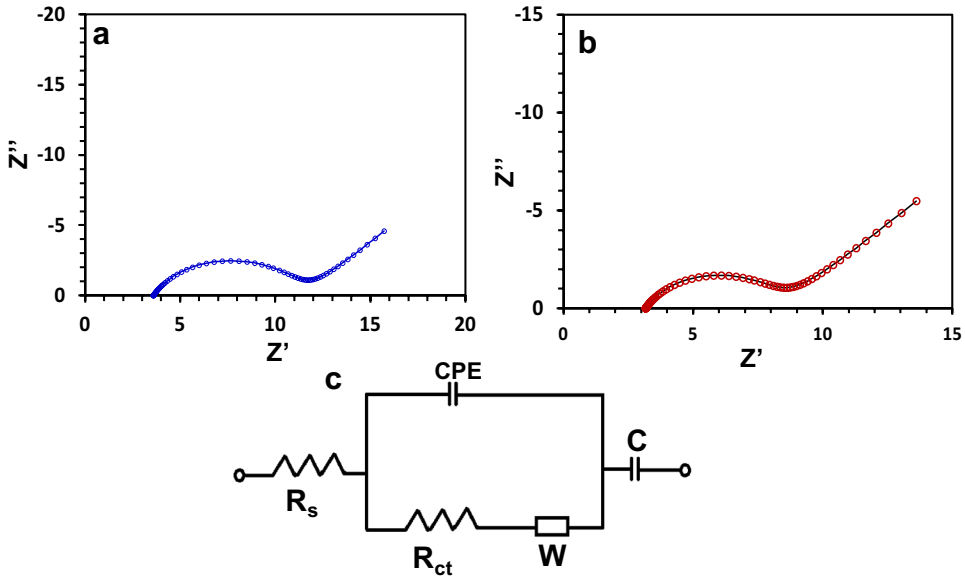

Fig. 8 EIS plot of **a** PANI/NiHCF/CF, **b** PANI/CoHCF/CF nanocomposite electrode, **c** fitting circuit of Nyquist plot

Table 3 Fitting data of equivalent circuit elements obtained by simulation of impedance spectra

Electrode	R_s (Ω)	R_{ct} (Ω)	$W_d \times 10^{-2}$ (Ω)	CPE $\times 10^{-3}$ (F)	C_p (F)	n
PANI/NiHCF/CF	3.18	7.67	20.4	0.8	7.67	0.7
PANI/CoHCF/CF	3.15	5.31	17.2	1.2	7.63	0.7

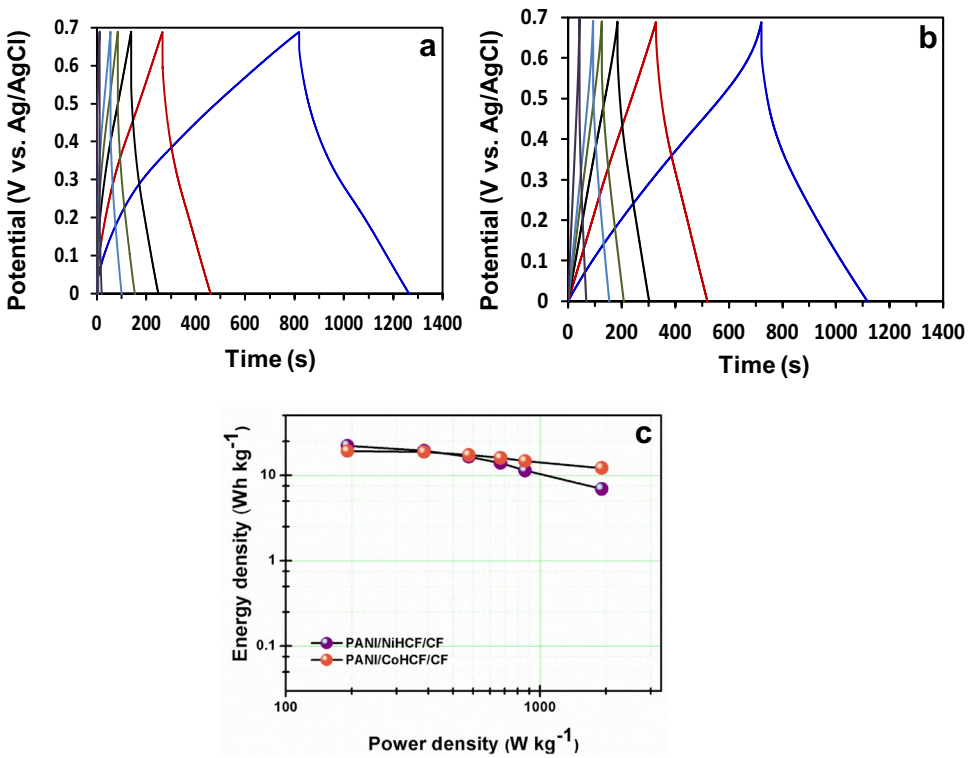

Fig. 9 Galvanostatic charge–discharge curves of symmetric supercapacitor consisting of **a** PANI/NiHCF/CF, **b** PANI/CoHCF/CF nanocomposite electrode at a current density of 0.5–5 A g^{-1} and **c** Ragone plot of symmetric supercapacitors

attributed to the intrinsic reversibility of PANI and MHCFs in the electrolyte. The calculated specific capacitances from the charge–discharge curves are 326, 285, 241, 204, 166, 63 F g^{-1} (PANI/NiHCF/CF) and 283, 274, 253, 234, 216, 179 F g^{-1} (PANI/CoHCF/CF) at 0.5, 1.0, 1.5, 2.0, 2.5, 5.0 A g^{-1} respectively. The electrochemical performances of the fabricated symmetric electrodes are also reflected by their energy and power densities, as shown in the Ragone plot (Fig. 9c). The maximum energy density (E_{max}) and power density (P_{max}) of the PANI/NiHCF/CF and PANI/CoHCF/CF electrodes were calculated to be 22.1 Wh kg^{-1} and 1.75 kW kg^{-1} and 19.2 Wh kg^{-1} and 1.75 kW kg^{-1}, respectively. Considering the capacitances of PANI/NiHCF/CF and PANI/CoHCF/CF electrodes obtained both in three-electrode and two-electrode systems, the electrodes can deliver with enhanced electrochemical performance. These results suggest the utility of these flexible devices in practical applications such as electric vehicles and wearable electronics.

4 Conclusions

A simple and fast approach for preparation of binder free flexible PANI/MHCF nanocomposites on carbon fibers electrodes was fabricated as a supercapacitor material. The MHCF nanoparticles can be uniformly interconnected to polyaniline in the CF surface. Their maximum specific capacitances of PANI/MHCF/CF nanocomposites were observed around 725 F g^{-1} at a current density of 1 A g^{-1}. Electrochemical tests revealed a notably high specific capacitance of PANI/MHCF/CF nanocomposite with high discharge densities, which makes the material to be a good candidate for energy applications. Hence, these superior properties of PANI/NiHCF/CF and PANI/CoHCF/CF nanocomposites will prompt their extensive use as the promising electrode materials for supercapacitors. These supercapacitors will be used in significant components in flexible devices. Finally, a low cost and rapid route for the fabrication of supercapacitors were achieved in this investigation.

Acknowledgements We would like to thank the financial supports by the Brazilian agencies such as CAPES (BEX 5383/15-3), (PNPD-PhD scholarships) CNPq and FAPERJ (E-26/110.087/2014, /213.577/2015 and /216.730/2015).

References

1. A.N. Menegaki, Renew. Energy **39**, 30–39 (2012)
2. P. Simon, Y. Gogotsi, Nat. Mater. **7**, 845–854 (2008)
3. Y.S. Luo, J.S. Luo, J. Jiang, W.W. Zhou, H.P. Yang, X.Y. Qi, H. Zhang, H.J. Fan, Y.W.Y. Denis, C.M. Li, T. Yu, J. Mater. Chem. A **1**, 273–281 (2013)
4. J. Yan, Q. Wang, C. Lin, T. Wei, Z. Fan, Adv. Energy Mater. **4**, 1400500 (2014)
5. P. Cheng, T. Li, H. Yu, L. Zhi, Z. Liu, Z. Lei, J. Phys. Chem. **120**, 2079–2086 (2016)

6. Y. Zou, S. Wang, Sci. Rep. **5**, 11792 (2015)
7. F. Shi, L. Li, X. Wang, C. Gu, J. Tu, RSC Adv. **4**, 41910–41921 (2014)
8. Z. Ma, X. Huang, S. Dou, J. Wu, S. Wang, J. Phys. Chem. C **118**, 17231–17239 (2014)
9. J. Wu, C. Ouyang, S. Dou, S. Wang, Nanotechnology **26**, 325401 (2015)
10. F. Zhao, Y. Wang, X. Xu, Y. Liu, R. Song, G. Lu, Y. Li, ACS Appl. Mater. Interfaces **6**, 11007–11012 (2014)
11. Y. Wang, Y. Yang, X. Zhang, C. Liu, X. Hao, J. Solid State Electrochem. **19**, 3157–3168 (2015)
12. H. Mi, J. Zhou, Q. Cui, Z. Zhao, C. Yu, X. Wang, J. Qiu, Carbon **80**, 799–807 (2014)
13. H.J. Buser, D. Schwarzenbach, W. Petter, A. Ludi, Inorg. Chem. **16**, 2704–2710 (1977)
14. M. Giorgetti, M. Berrettoni, Inorg. Chem. **47**, 6001–6008 (2008)
15. J. Chen, K. Huang, S. Liu, Electrochem. Commun. **10**, 1851–1855 (2008)
16. Z. Wang, S. Sun, X. Hao, X. Ma, G. Guan, Z. Zhang, S. Liu, Sens. Actuators B **171–172**, 1073–1080 (2012)
17. R.S. Babu, P. Prabhu, S.S. Narayanan, J. Chem. Pharm. Res. **4**, 3592–3600 (2012)
18. H. Jiang, Y.-T. Xu, T. Wang, P.-L. Zhu, S. Yu, Y. Yu, X.-Z. Fu, R. Sun, C.-P. Wong, Electrochim. Acta **166**, 157–162 (2015)
19. S. Ghasemi, S.R. Hosseini, P. Asen, Electrochim. Acta **160**, 337–346 (2015)
20. H. Wang, J. Lin, Z.X. Shen, J. Sci. Adv. Mater Dev. **1**, 225–255 (2016)
21. P.J. Kulesza, K. Miecznikowski, M.A. Malik, M. Galkowski, M. Chojak, K. Caban, A. Wieckowski, Electrochim. Acta **46**, 4065–4073 (2001)
22. P.A. Fiorito, S.I.C. de Torrsei, J. Electroanal. Chem. **581**, 31–37 (2005)
23. P.J. Kulesza, K. Miecznikowski, M. Chojak, M.A. Malik, S. Zamponi, R. Marrasi, Electrochim. Acta **46**, 4371–4378 (2001)
24. D. Ellis, M. Eckhoff, V.D. Neff, J. Phys. Chem. **85**, 1225–1231 (1981)
25. J.B. Ayers, W.H. Waggoner, J. Inorg. Nucl. Chem. **33**, 721–733 (1971)
26. K. Itaya, I. Uchida, V.D. Neff, Acc. Chem. Res. **19**, 162–168 (1986)
27. A. Safavi, S.H. Kazemi, H. Kazemi, Electrochim. Acta **56**, 9191–9196 (2011)
28. N.K.A. Venugopal, J. Joseph, J. Power sources **305**, 249–258 (2016)
29. H. Pang, Y. Zhang, T. Cheng, W.-Y. Lai, W. Huang, Nanoscale **7**, 16012–16019 (2015)
30. Y. Yang, Y. Hao, J. Yuan, L. Niu, F. Xia, Carbon **84**, 174–185 (2015)
31. R. Kotz, M. Carlen, Electrochim. Acta **45**, 2483–2498 (2000)